Microstructure and abrasive wear properties of M(Cr,Fe)$_7$C$_3$ carbides reinforced high-chromium carbon coating produced by gas tungsten arc welding (GTAW) process

[1]Soner BUYTOZ*, [2]M.Mustafa YILDIRIM

[1]University of Fırat, Faculty of Technical Education, Department of Metallurgy, Elazig, 23119 TURKEY
[2]University of Dumlupinar, Department of Mechanical Engineering, Kutahya, TURKEY
Corresponding: * sbuytoz@firat.edu.tr

Abstract

In the present study, high-chromium ferrochromium carbon hypereutectic alloy powder was coated on AISI 4340 steel by the gas tungsten arc welding (GTAW) process. The coating layers were analyzed by optical microscopy, X-ray diffraction (XRD), field-emission scanning electron microscopy (FE-SEM), X-ray energy-dispersive spectroscopy (EDS). Depending on the gas tungsten arc welding parameters, either hypoeutectic or hypereutectic microstructures were produced. Wear tests of the coatings were carried out on a pin-on-disc apparatus as function of contact load. Wear rates of the all coating layers were decreased as a function of the loading. The improvement of abrasive wear resistance of the coating layer could be attributed to the high hardness of the hypereutectic M$_7$C$_3$ carbides in the microstructure. As a result, the microstructure of surface layers, hardness and abrasive wear behaviours showed different characteristics due to the gas tungsten arc welding parameters.

Keywords: TIG process; abrasive wear; M$_7$C$_3$ carbide.

1. Introduction

Iron based surface coating is very popular and their resistance to wear is due to the hard carbides distributed in a relatively soft matrix. Earlier researches on Fe-Cr-C alloys using methods such as laser and plasma it was seen that complex carbides with rich chromium such as M(=Cr, Fe)$_3$C, M(=Cr, Fe)$_7$C$_3$ and M(=Cr, Fe)$_{23}$C$_6$ and microstructures which were the mixture of α-ferrite were formed depending on the chemical composition of the alloy [1-3]. This type of microstructures showed good abrasive wear resistance [4,5]. However, in all of these investigations, microstructures with primary carbides relatively larger were obtained in comparison with those obtained by rapid solidification methods. Improve the properties of Fe-Cr-C can used TIG method [6,7].

Hardfacing by means of TIG welding method associated with a rapid heating and cooling rate provided a unique opportunity for the non-equilibrium synthesis of materials and produced rapidly solidified fine microstructures with extended solid solution of alloying elements [8], thus providing remarkable enhancement on corrosion resistance [9], wear resistance [10] and thermal conductivity without impairing the bulk properties. In the surface coating applied, being the new and an easy method which makes the new compositions deeper, fine grained and intermetallic compound, hardness of the material can increase the capacities of wear resistance, fatigue resistance, fracture resistance and load carrying capacity [11-13]. Process TIG can be used for surface alloying to increased fatigue strength, increased resistance to long-term load at high temperatures (creep test) [14].

This paper introduces to Fe based hypereutectics and hypoeutectics coatings with high-chromium forming on AISI 4340 steel by the tungsten inert gas (TIG) process. The microstructure, microhardness and wear rate of the surface layers were studied to determine appropriate compositions as well as determining suitable TIG parameters such as powder content, heat input value and scan speed.

2. Experimental procedures

In this study, high-chromium ferrochromium carbon hypereutectic alloy powder was used as coating material on AISI 4340 steel (100×20×10 mm) by the tungsten inert gas (TIG) process. The schematic representation of tungsten inert gas welding method is shown in Figure 1 (a). Its chemical composition in wt.% is 0.4 15% C, 0 .267% Si, 0.656% Mn, 1.75% Ni, 0.237% Mo, 0.930% Cr and 95.54% Fe . However, the powders used in the experiments consist of 64% Cr, 1. 80% Si, 6. 84% C and 26.84% Fe.

(a)

(b)

(a): Height of coating plate, mm
(b): Width of coating plate, mm
(c): Length of coating plate, mm
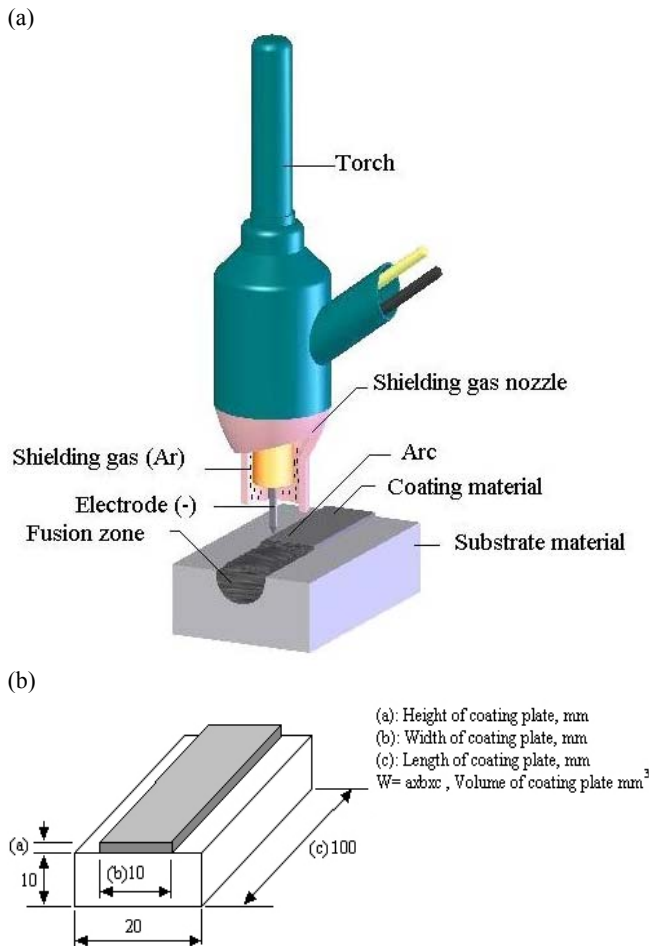$W = a \times b \times c$, Volume of coating plate mm^3

Fig. 1. Schematic representation (a) of the coating process and (b) of coating sample

The alloying was carried out with the two-step method. Initially, the sample surface was polished with 400 grit SiC paper then the mixed powder layers of a thickness of about 1.0–3.0 mm were preplaced on the surface of the substrate with small amoun t of alcohol, and then the substrates with this coating were dried in furnace at a temperature of 50 ºC for 120 min. It enabled to keep the powder layers on the surface under the flow of argon during the arc melting and to vaporize the chemical binder before treatment. The schematic picture of coating sample can be seen in Figure 1 (b). Subsequently, the coating was melted using the TIG weld method. The electrode was 2% thoriated tungsten and the nozzle diameter was 11 mm. To avoid the oxidation of the alloyed coating, and to provide a relatively inert environment, argon was blown directly into the molted pool and to the processing region. Experiments were carried out wi th a single track. The experiment conditions are shown in Table 1 and Table 2, respectively. The heat input values were calculated as

$$Q = \eta \frac{U.I}{V} \qquad (1)$$

where, Q: heat input, η: welding efficiency (0.7), U: voltage (V) and I: current (A) and V: welding speed (mm/s). The gas tungsten arc welding parameters, i.e. heat input values were fixed at between 12.1 and 14.1 kJ/cm. Two process speed values of 1.17 mm/s for sample S_1 and 1.44 mm/s for sample S_4 were selected. The coatings were carried out on the AISI 4340 steel which powder layers having the weight of 3.5 g and 5 g were preplaced on the surface. The dilution values were as

$$Dilution = \frac{A_1}{(A_1 + A_2)} \qquad (2)$$

where, A_1: cross-sectional area of the penetration zone of the parent metal, A_2: cross-sectional area of the deposit (above the original surface), $A_1 + A_2$: coating thickness.

Table 1. Process parameters

Process speed	1.174-1.438 mm/s
Electrode diameter	2.4 mm
Powder content	3.5-5 g
Heat input[*]	12.1-14.1 kJ/cm
Current/Volt	120 A/20 V
Electrode	2% thorium tungsten electrode
Shielding gas	99.9% pure Ar
Gas flow rate	11 l/min

Samples for metallographic examinations were taken from the cross section to the modification surface from the coating areas. The metallographic specimens were grinded with 80-1200 mesh sandpaper; the grinded surfaces were cleaned and then polished with 1 and 6 μm diamond paste and solvent. The polished specimens were etched with acidic ferric chloride solution (25 grams of $FeCl_3$, 15 ml of HCl and 100 ml of distilled water). The microstructures of the surface layers were observed by scan-

ning electron microscope (SEM), energy dispersive spectrograph (EDS) and X-ray diffraction (XRD). XRD analyses were done by using Cu-Kα radiation in 30 kV and 15 mA with Rigaku Geiger-flex X-ray diffractometer.

Table 2. Operation conditions and geometrical characteristics of the coating

Process parameters				Coating dimensions (mm)				
S. no	Powder type	Scan speed (mms^{-1})	Heat input (kJ.mm^{-1})	A_1	A_2	A_1+A_2	Dilution	Hardness (HV)
S_1		1.17	14.3	2.61	1.08	3.69	0.70	764±48
S_2	FeCrC powder	1.29	14.1	1.85	1.33	3.38	0.54	861±60
S_3		1.33	13.7	1.35	1.15	2.50	0.54	808±21
S_4		1.44	12.1	0.75	0.97	1.72	0.43	712±31

Abrasive wear experiments were carried out at the room temperature and normal atmosphere conditions with dry sliding pin-on-disc experiment apparatus. Fig. 2 shows a schematic diagram of the wear test apparatus. Prior to wear experiments, each sample was exposed to 1200 mesh sandpaper for the contact completely to the 80 mesh paper coated abrasive disk surface. In the experimental procedure, three different loads of 10, 20 and 30 N were selected at total sliding distance of 60 meter. After each experiment, 80 mesh abrasive sandpapers were changed. Abrasive wear rates were recorded by determining the weight losses of the samples prior and after the tests.
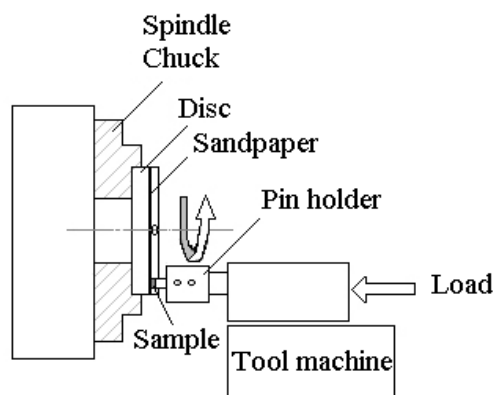

Fig. 2. A schematic view of the abrasive test apparatus

3. Results and Discussion

3.1. Microstructure

The microstructures of surface layers are given in Fig. 3. The porosity and cracks were not found in the surface layers. When the microstructures of the surface layers were examined that had been modified with tungsten inert gas welding method, depending on the TIG process parameters they were seen to be solidified in the microstructures consisting of carbides and phases in different compositions and quantities.

Specifically, as a function of the heat input and powder content, the microstructure of the sample S_1 which was produced in the 14.3 kJ/cm heat input, 3.5 g powder content and 1.174 mm/s scan speed exhibited a fine grained dendrite solidification along the depth of coating substrate (Fig. 3a). However, reducing the heat input and increasing of the powder content produced at the different microstructures in samples S_2–S_4 composing of primary phases and eutectic (Fig. 3b-d). As reveals in Figure 3b [8], the coating consist of large primary M(=Cr, Fe)$_7$C$_3$ carbides and eutectic (γ+M(=Cr, Fe)$_7$C$_3$) structure. This structure mechanism is features of hypereutectic structure [15,16]. However, it was observed according to EDS data that solidification was formed hypoeutectically for sample S_1 (Table 3). As shown in Fig. 4, XRD patterns indicate the presence of respective carbides in the surface layers. These primary carbides are also assumed to be M(Cr,Fe)$_7$C$_3$ carbides (Fig. 3b), consistent with the EDS analysis results given in Table 3. The hexagonal and rod-shaped primary M(Cr,Fe)$_7$C$_3$ carbides has been surrounded by the eutectic austenite (γ) with relatively low chromium and carbon elements (see Fig. 3c and d). The primary M(=Cr,Fe)$_7$C$_3$ carbide is the first phase to form on cooling below the liqudius temperature and residual liquid should decompose an eutectic reaction into austenite and M(=Cr,Fe)$_7$C$_3$ eutectic carbides [17]. The results of XRD and EDS show that there are two different structures formed in all samples. First structure mechanism is formed of dendrite shaped austenite having eutectic structure composed of austenite containing M(Cr, Fe)$_7$C$_3$ carbides in the samples S_1 which had approximately less carbon content than 4% C [18].

Second structure mechanism is the formation of primary M(Cr,Fe)$_7$C$_3$ carbides and hypereutectic microstructure having austenitic eutectic structure (Fig. 3b-d). This mechanism was formed in the sample S_3- sample S_4 this had more carbon concentration than 4% C. Although hypereutectic microstructures contain more carbide, they show different microstructures depending on the different welding characteristics and cooling rate [19].
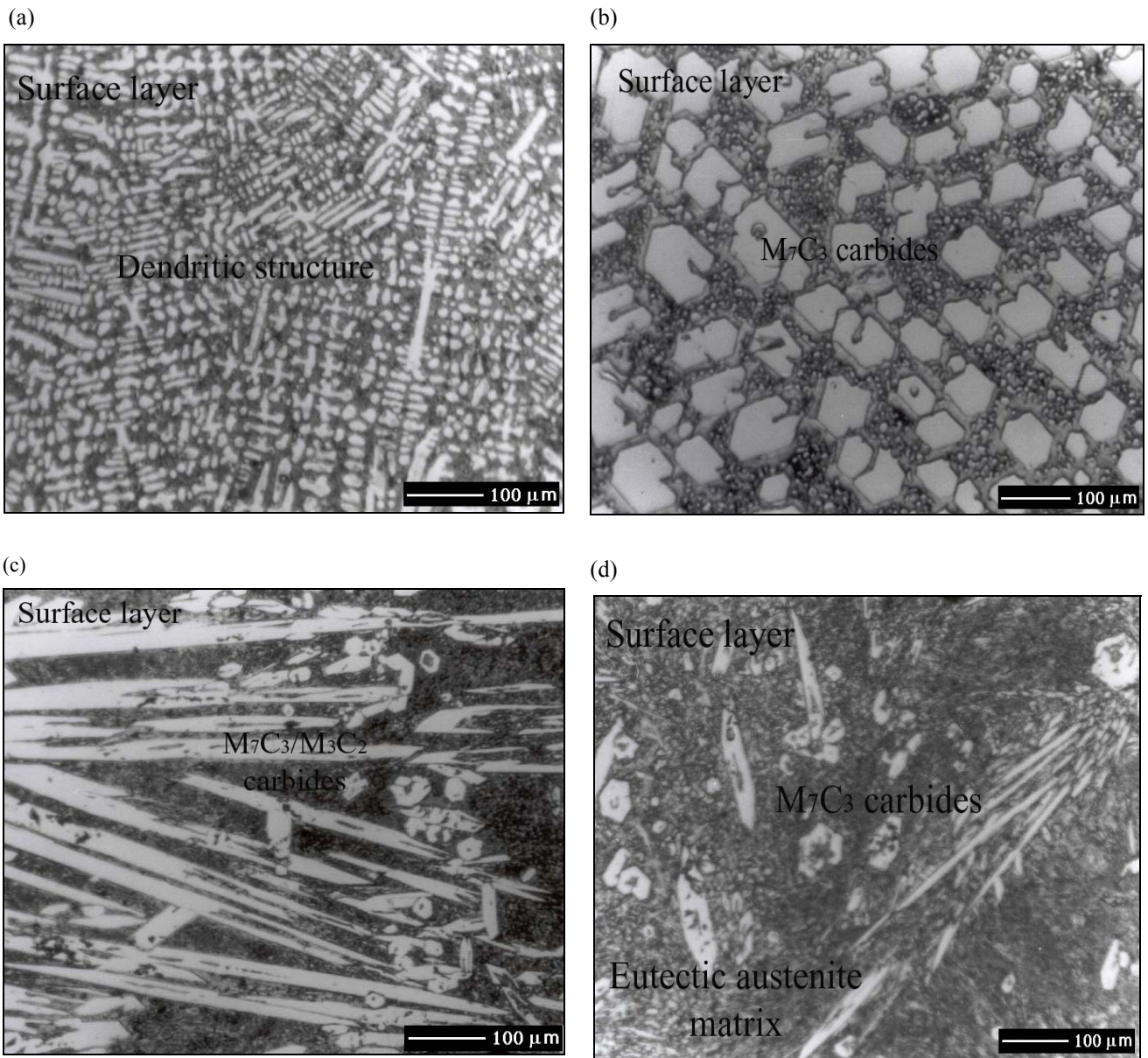
(a)

(b)

(c)

(d)

Fig. 3. Optical micrographs of (a) showing surface layer of sample S_1, (b) surface layer of sample S_2, (c) surface layer of sample S_3 and (d) surface layer of sample S_4

3.2. Hardness

Mechanical and tribological properties of the coatings depend on concentration of alloy elements, type of the solidified phases and distribution of the hard carbides [20]. M(Cr, Fe)$_7$C$_3$ carbides are relatively harder carbides than (α) ferrite, austenite (γ) and M(Cr, Fe)$_3$C carbides [21].

Hardness values taken from the samples S_1-S_4 are given in Table 2. Debt of the surface layers and dilution ratio of all samples can be also seen Table 2. During the surface modification, a significant melting of base material was obtained accord-

ing to TIG parameters such as decreasing powder content and increasing heat input values. It can be seen from the Table 2 that maximum hardness was determined for sample S_2 owing to relatively high heat input and low scan speed. However, although an instantaneous increase was observed in the hardness in the interface regions of the sample S_3, there was a decrease in this value towards the substrate of the sample S_4. This is due to the density of the carbides and phases which are formed depending on the different solidification rates in the intermediate rate. When the carbide content increased, there was an increase in the hardness. The hardness values demonstrate that significant

hardfacing has been achieved by means of tungsten inert gas method. In this connection, the surface modification with the gas tungsten arc method is changed to the surface properties of the substrate material, i.e. the chemical composition, surface roughness, toughness, wear and corrosion [4]. The hardness of coatings improved with the tungsten inert gas method is higher than other melt methods such as GMA weld and submerged arc weld [22]. Because distribution of the carbides in both eutectic and primary phase and homogenous distribution of solidified austenite (γ) phase make them harder [23].

Table 3. EDX analysis results of phases and carbides in the TIG processed coating microstructures

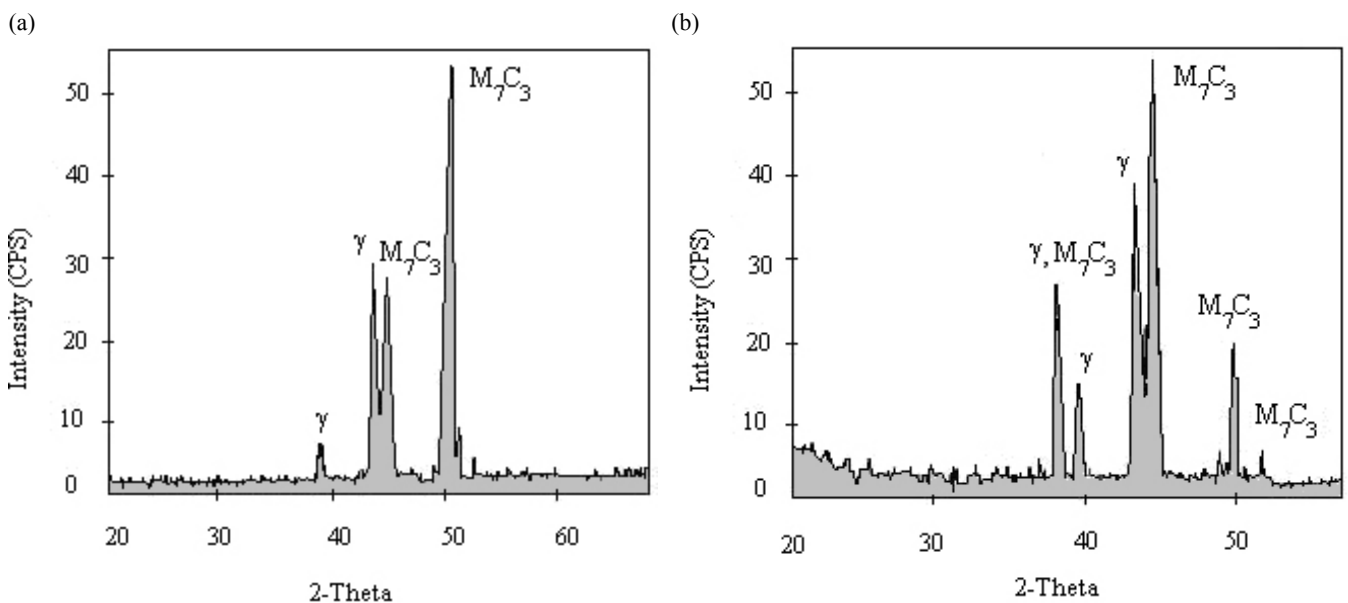| Sample number	Area	Structure	Cr	C	Si	Fe	Other
S_1	Matrix	Hypoeutectic	14.0	3.35	1.07	80.5	1.53 Ni
	phase	Dendrite	30.54	7.86	-	60.28	-
S_2	Matrix	Hypoeutectic	10.36	3.60	0.76	85.28	-
	Carbide	Primary M_7C_3	48.83	8.08	-	40.63	2.46 Mo
S_3	Matrix	Hypereutectic	35.05	9.62	0.81	53.68	-
	Carbide	$M_7C_3 + M_3C_2$	65.97	9.66		27.15	-
S_4	Matrix	Hypereutectic	40.83	10.14	0.82	47.57	0.63
	Carbide	Primary M_7C_3	81.97	9.18	-	8.85	-

(a)

(b)

Fig. 4. XRD pattern of (a) sample S_1 having hypoeutectic structure, (b) sample S_2 having hypereutectic structure

3.3. Abrasive wear

The change of wear rate curves under different loadings are given in Fig. 5. The wear rate values were calculated by dividing the weight loss emerged as a result of the load applied by distance. It can be seen that the lowest and highest wear rates are obtained from the sample S_2 and sample S_4, respectively. The samples S_1 and S_3 drew a similar inclination. This samples are having to hypereutectic microstructures that they are more

consist of M(=Cr, Fe)$_7$C$_3$ eutectic carbide and phases. M(Cr,Fe)$_7$C$_3$ carbides were one of the typical phases formed in the Fe, Cr, and C concentration alloys [19,20]. In Table 3 and Fig. 5, it can be seen that although these carbides which played significant roles in the hardness of the matrix material were hard, it significantly increased the wear performance of the surface layers. It is stated in the literature that the load applied during the process of wear is carried to the strengthening ele-

ments by the matrix and as a result the wear rate diminishes [21-25].

The relation of the hardness values to total weight loss shows for total sliding distance 60 m in Fig 6. According to Fig. 6, the sample S_1 with 764 HV hardness value lost 2.45 g under abrasive wear test condition. However, the weight loss of the sample S_2 was determined 1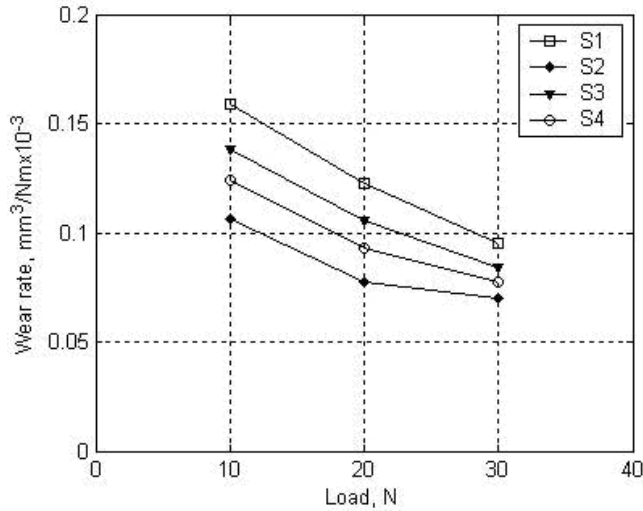.65 g and there was a fall recorded in the weight loss when compared to that of the samples S_3 and sample S_4. This data indicate that the finely dispersed distribution in the matrix and rates of the primary hard carbides $(M(Cr,Fe)_7C_3)$ in the microstructure causes the hardness values to be high and as a result it directly affects the wear, as shown by Buchely et al. [20].
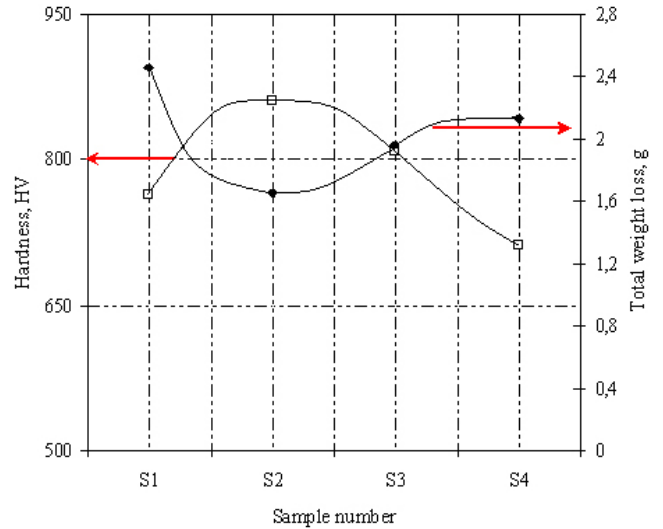

Fig. 5. Variations of abrasive wear rate as a function of load

Fig. 6. Relationship between weight loss and average hardness values

The morphologies of the worn surface of sample S_1 - sample S_4 for the FeCrC coatings are shown in Fig. 7. It can be seen that the debris depth formed in the sample S_2 after wear was slighter than those of the samples S_1, S_3 and sample S_4. Also, the worn surface of sample S_2 is shallow and long continuous grooves (Fig. 7b). On the contrary, the worn surface of sample S_1 approximately 0.5-1.5 times narrower tracks than the samples S_3 and S_4, as shown in Fig. 7a, Fig. 7c and Fig. 7d, respectively. It can be established that variations in wear rate are related to the difference in hardness of the surface layers. When the abrasives particles exhibit the hardness greater than 4 times than that of the wearing matrix material, the abrasive particles can penetrate easily to the sample, thereby causing microploughing and microcutting within the wearing surface [26].

4. Conclusion

In this study, the abrasive wear behaviour of FeCrC coatings were investigated at different loads. The following results have been found:

In the microstructures of the surfaces alloyed with high-chromium ferrochromium carbon powders, depending on the concentration of alloy elements, specifically C and Cr concentration, hypoeutectic and hypereutectic microstructures have been observed. In high heat input and low powder contents, the microstructure containing hypoeutectic, eutectic interdendrites, and austenite phases and carbides has been obtained. Due to the low amounts of C and Cr in the structure and presence of the primary dendritic austenite structure together with the eutectic structure formation, relatively lower hardness values have been recorded. However, in the hypereutectic structures, higher hardness values were determined because of the presence of the hypereutectic microstructure consisting of primary $(M(Cr,Fe)_7C_3)$ carbides and austenite. The hypereutectic microstructure consisted of $(M(Cr,Fe)_7C_3)$ and $(M(Cr,Fe)_7C_3)$ + austenite (γ) at present process conditions.

In the samples to which high-chromium ferrochromium carbon surface modification applied, the best wear behaviour is recorded at different loadings in sample S_2 which the primary $(M(Cr,Fe)_7C_3)$ carbides are finely dispersed distribution in matrix.
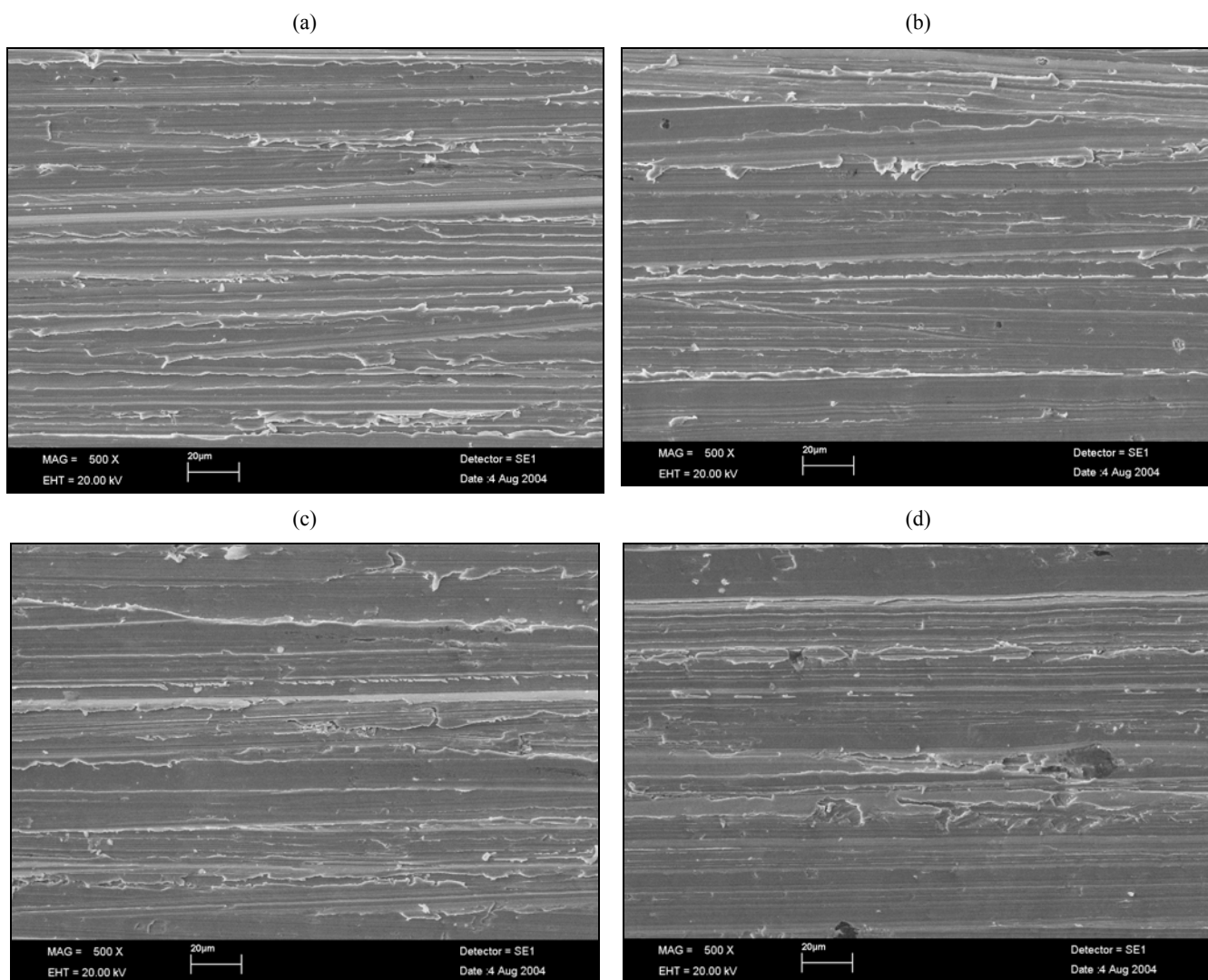
(a)

(b)

(c)

(d)

Fig.7. SEM micrographs of worn surfaces of (a) sample S_1, (b) sample S_2, (c) sample S_3 and (d) sample S_4

References

[1] Q.Y. Hou, J.S. Gao, F. Zhou, Microstructure and wear char-acteristics of cobalt-based alloy deposited by plasma trans-ferred arc weld surfacing, Surface and Coatings Technology 194 (2005) pp. 238-243

[2] H.-N. Liu, M. Sakamoto, M. Nomura, K. Ogi, Abrasion resistance of high Cr cast irons at an elevated temperature, Wear 250 (2001) pp. 71-75

[3] S. Buytoz, Microstructural properties of M_7C_3 eutectic car-bides in a Fe–Cr–C alloy, Materials Letters 60 (2006) pp. 605-608

[4] S. Buytoz, Ph.D. Thesis, Firat University, Elazig 733 (2004) Turkey.

[5] H. Berns, Comparison of wear resistant MMC and white cast iron, Wear 254 (2003) pp. 47-54

[6] Trytek A., Orłowicz A.: The thermal efficiency and melting efficiency of the fusion process on cast iron with Cr. Archives of Foundry vol. 6, nr 18 (2/2), 319-324, 2006

[7] Orłowicz A., Trytek A.: Surface melting of cast iron alloy with chromium: Archives of Foundry vol. 6, nr 18 (2/2), 313-318, 2006

[8] S. Buytoz, M.M. Yildirim, H. Eren, Microstructural and microhardness characteristics of gas tungsten are synthe-sized Fe–Cr–C coating on AISI 4340, Materials Letters 59 (2005) pp. 607-614

[9] M. Hadad, R. Hitzek, P. Buergler, L. Rohr and S. Siegmann, Wear performance of sandwich structured WC–Co–Cr thermally sprayed coatings using different intermediate lay-ers, Wear263 (2007) pp. 691-699.

[10] H.M. Wang, C.M. Wang, L.X. Cai, Wear and corrosion resistance of laser clad $Ni_2Si/NiSi$ composite coatings, Surface and Coatings Technology 168 (2003) pp. 202-208.

[11] F.T. Cheng, K.H. Lo, H.C. Man, NiTi cladding on stainless steel by TIG surfacing process: Part I. Cavitation erosion behavior, Surface and Coatings Technology 172 (2003) pp. 308–315.

[12] Mróz M., Orłowicz A., Tupaj M.: Influence of structural parameter λ_{2D} dendrites α-phase on the wear intensity of C355 alloy casting after surfacing process with concentrated beam heat. TRIBOLOGIA. TEORIA I PRAKTYKA, vol. 39, nr 1, 101-109, 2008.

[13] Mróz M., Orłowicz A., Tupaj M.: Fatigue of C355 alloy after rapid solidification. Archives of Foundry vol. 5, nr 15, 271-277, 2005

[14] Orłowicz A.W., Trytek A., Opiekun Z., Mróz M., Mesko J.: Form remelting of castings alloy MAR-M 509 using plasma electric arc. XXXVII International conference a diskusne forum: ZVARANIE 2009 - Welding 2009. Sloveska zvaracska spolocnost. Taranska Lomnica 04-06.11.2009, 148-153

[15] K. Nagarathnam, K. Komvopoulos, Microstructural and microhardness characteristics of laser-synthesized Fe-Cr-W-C coatings, Metall. Mater. Trans A26 (1995) pp. 2131-2139.

[16] H.-J. Kim, S. Grossi, Y.-G. Kweon, Wear performance of metamorphic alloy coatings, Wear 232 (1999) pp. 51-60.

[17] H. Berns, A. Fischer, Microstructure of Fe-Cr-C Hardfacing alloys with additions of Nb, Ti and, B, Materials Characterization 39 (1997) pp. 499-527.

[18] L. Lu, H. Soda, A. McLean, Microstructure and mechanical properties of Fe–Cr–C eutectic composites, Materials Science and Engineering A 347 (2003) pp. 214-222

[19] C. G. Schön, A. Sinatora, Simulation of solidification paths in high chromium white cast irons for wear applications, Calphad 22 (1998) pp. 437-448

[20] H. K. D. H. Bhadeshia, L. -E. Svensson and B. Gretoft, A model for the development of microstructure in low-alloy steel (Fe-Mn-Si-C) weld deposites, Acta Metallurgica 33 (1985) pp. 1271-1283

[21] S.G. Sapate, A.V. Rama Rao, Effect of carbide volume fraction on erosive wear behaviour of hardfacing cast irons, Wear 256 (2004) pp. 774–786

[22] B.Gulenc, N. Kahraman, Wear behaviour of bulldozer rollers welded using a submerged arc welding process Materials and Design, 24 (2003) pp. 537-542

[23] D.V. Shtansky, K. Nakai, Y. Ohmori, Crystallography and interface boundary structure of pearlite with M_7C_3 carbide lamellae, Acta Mater. 47 (1999) pp. 1105-1115

[24] C. K. Kim, S. Lee, J.-Y. Jung, S. Ahn, Effects of complex carbide fraction on high-temperature wear properties of hardfacing alloys reinforced with complex carbides, Materials Science and Engineering A 349 (2003) pp. 1-11

[25] M.F. Buchely, J.C. Gutierrez, L.M. Le´on, A. Toro, The effect of microstructure on abrasive wear of hardfacing alloys, Wear 259 (2005) pp. 52-61

[26] S.C. Tjong, K.C. Lau, Abrasion resistance of stainless-steel composites reinforced with hard TiB_2 particles, Composites Science and Technology 60 (2000) pp. 1141-1146